Quantitative interpretation of electron-beam-induced current grain boundary contrast profiles with application to silicon

Richard Corkish,[a] Tom Puzzer, and A. B. Sproul
Photovoltaics Special Research Centre, University of New South Wales, Sydney 2052, Australia

Keung L. Luke
Department of Physics and Astronomy, California State University, Long Beach, California 90840

(Received 19 March 1997; accepted for publication 13 August 1998)

An improved method is described for extracting material parameters from an experimental electron-beam-induced current (EBIC) contrast profile across a vertical grain boundary by directly fitting an analytical expression. This allows the least-squares values of the grain boundary recombination velocity and the diffusion length in each grain to be determined without the need for the reduction of the experimental profile to a few integral parameters, as is required in a previously reported method. Greater accuracy of the extracted values is expected since none of the information contained in the experimental contrast data is discarded and a less extensive spatial range of measured data is required than in the commonly used method. Different models of the carrier generation volume are used in the fitting and the effect of the choice of generation model on extracted values is investigated. In common with other EBIC approaches, this method is insensitive to changes in the diffusion length when the collection efficiency is high and diffusion lengths may not be reliably established in those cases. © *1998 American Institute of Physics.*
[S0021-8979(98)02722-4]

I. INTRODUCTION

The need for the adoption of alternatives to semiconductor-grade material by the solar cell industry is a major incentive for much of the current solar cell research. Alternatives[1] offer the advantages of reduced energy investment[2] and financial cost at the expense of lower energy conversion efficiency. Cells made of cast silicon and various amorphous and polycrystalline semiconductors are now routinely manufactured. In solar cells and other devices made from multicrystalline or polycrystalline materials, the recombination of minority carriers at grain boundaries is a critical limitation on their performance.[3,4] Researchers and manufacturers need methods to quantify grain boundary parameters in experimental and production devices in order to be able to ascertain the impact of grain boundaries on device performance and to measure the effectiveness of grain boundary passivation techniques,[5] which are intended to mitigate their impact.

It has been shown by Donolato[6] that an expression may be derived to describe the variation of electron- or light-beam-induced current (EBIC or LBIC) contrast across a semiconductor grain boundary in terms of two parameters: L, the diffusion length within the grain and s, which is defined as the grain boundary recombination velocity, v_s, divided by the diffusivity of the minority carriers, D. In order to obtain such an expression, Donolato made the following assumptions: (i) that generation and recombination of charge carriers could be neglected in the emitter layer (if carrier collection is by a p-n junction) and in the junction depletion region (this implies a beam acceleration voltage high enough to ensure deep generation); (ii) that both the plane of the grain boundary and the electron beam are normal to the collecting junction (Fig. 1); (iii) that L is uniform, at least within each grain; (iv) that the grain boundary may be simply described as a planar interface with a particular recombination velocity which is independent of injection level; and (v) that the diffusion length is the same either side of the grain boundary. Donolato's expression for the contrast when the beam position is a distance x_0 from a grain boundary is[7]

$$c(x_0)=\frac{[I_0-I(x_0)]}{I_0}=\frac{2s}{I_0\pi}\int_{k=0}^{\infty}\left(\frac{k}{\mu^2(2\mu+s)}\int_{z=0}^{\infty}\left\{\sin(kz)\times\int_{x=-\infty}^{\infty}[\exp(-\mu|x|)h(x_0-x,z)]dx\right\}dz\right)dk, \tag{1}$$

where I_0 is the background current at a large distance from a grain boundary, $I(x_0)$ is the beam-induced current in the vicinity of a grain boundary, $\mu=(k^2+L^{-2})^{1/2}$, k is an integration variable, x is the lateral distance from the grain boundary, (x_0-x) is the lateral position relative to the beam location (see Fig. 1), and h is the projection of the generation volume, $g(x,y,z)$, onto the x,z plane,[8]

$$h(x_0-x,z)=\int_{-\infty}^{\infty}g(x_0-x,y,z)dy. \tag{2}$$

The background current may be found from[9]

[a]Electronic mail: r.corkish@unsw.edu.au

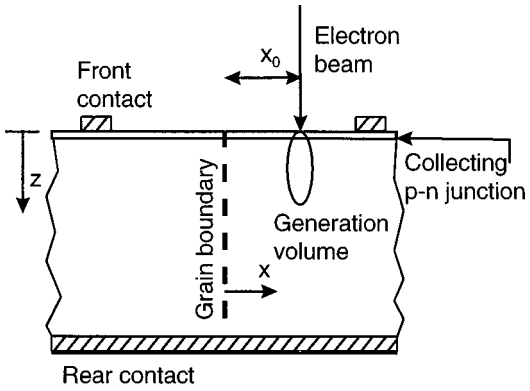

FIG. 1. Geometry of the electron-beam-induced current method used in this work.

$$I_0 = \int_0^\infty \left\{ \exp(-z/L) \int_{-\infty}^{\infty} [h(x_0 - x, z)]\, dx \right\} dz.$$

Equation (1) could be fitted to experimentally determined EBIC or LBIC contrast profiles by numerous evaluations within an optimization loop. However, Donolato described a faster procedure which involves the description of the profile by two integral parameters: its area and variance. His procedure has been used elsewhere.[5,10–12] Mittiga and Cappizzi[13] described an alternative, rapid technique for fitting Eq. (1) to experimental LBIC profiles. Their method uses the Fourier transform of the profile and does not require the reduction of the profile shape information to a few integral parameters. An analogous method for EBIC profiles has not appeared in the literature.

One concern with the integral-parameter method is that a very long series of EBIC data is required to accurately establish the variance parameter. The variance is defined[6] as

$$\Sigma^2 = A^{-1} \int_{-\infty}^{\infty} x_0^2 c(x_0)\, dx_0, \tag{3}$$

where A is the area under the contrast profile. The presence of the x_0^2 term in the integrand means that practical limits for the integral need to be very large in order to obtain convergence. On the other hand, contributions to the area integral rapidly become negligible as x_0 increases. Figure 2 shows the convergence of A and Σ, each normalized to the electron range, R, as the upper limit of integration is increased. For the purposes of this calculation, the lower limit was set to zero and the following parameter values were assumed: $L = 150\ \mu$m, $vs = 4.5 \times 10^5$ cm s^{-1}, $D = 30$ cm^2 s^{-1}, and $R = 6.6\ \mu$m. The area parameter, A/R, rapidly approaches its true value of 1.847 with integration up to $x_0 \approx 200\ \mu$m but the integration for Σ/R must be extended to $x_0 \approx 800\ \mu$m or beyond in order to closely approach an accurate result of 9.810. This demonstrates that great care must be taken to ensure that sufficient data are measured, or at least extrapolated, to permit an accurate estimate of the variance. The need for data far from the grain boundary has previously been noted by Mittiga and Capizzi. This effect is particularly important since the lack of a feedback mechanism in the graphical method could make it difficult for an erroneous value to be detected.

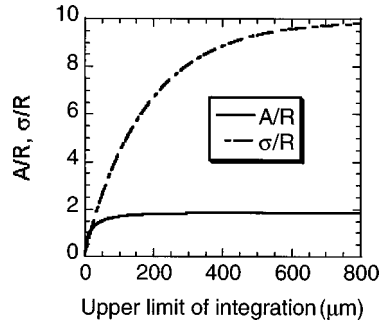

FIG. 2. Convergence of the integral parameters used in Donolato's graphical method as functions of the upper limit of integration.

In this work we describe a method of directly fitting Eq. (1) to experimental EBIC contrast profiles and apply it to a grain boundary in a silicon solar cell. With an appropriate model for the generation profile and taking advantage of modern computing speed, it is now a practical proposition to fit directly to Eq. (1) using a personal computer. At least one previous attempt has been made at direct fitting to EBIC grain boundary scans. Seager[14] fitted to the EBIC data an expression derived by Zook[15] for the LBIC response to an infinitesimally small laser beam by estimating an effective optical absorption coefficient for an electron beam. It will be shown that our more sophisticated analysis results in much closer agreement between theory and experiment. Masri *et al.*[16] estimated the diffusion length before fitting Marek's[17] model for the LBIC response to experimental grain boundary profiles in order to determine the grain boundary recombination velocity. Direct fitting avoids the compromise inherent in Donolato's technique in that we do not need to discard any information about the shape of the contrast profile. Additionally, our method provides direct feedback which allows the user to judge the reliability of the extracted values and our method does not necessarily require the EBIC profile to be measured as far from the grain boundary as is required in the integral parameter method, although good-quality data over long scan distances will generally improve the reliability of our method.

Zook's, Donolato's, and similar methods have been criticized on the grounds that the diffusion length values so determined have been found to be extremely sensitive to the procedure used to determine the baseline (i.e., The EBIC or LBIC response expected an infinite distance from the grain boundary) of the experimental profile.[10,18] The method presented here allows higher reliability in determining the grain boundary recombination velocity. However, in common with any other EBIC method, ours is essentially insensitive to changes in diffusion length when the carrier collection efficiency is high.

II. THEORY

A. Models for the generation volume

A large number of approximations have appeared in the literature for the supposed distribution of electron-hole pair generation within a sample under the influence of electron beam radiation. In this work we have made use of four dif-

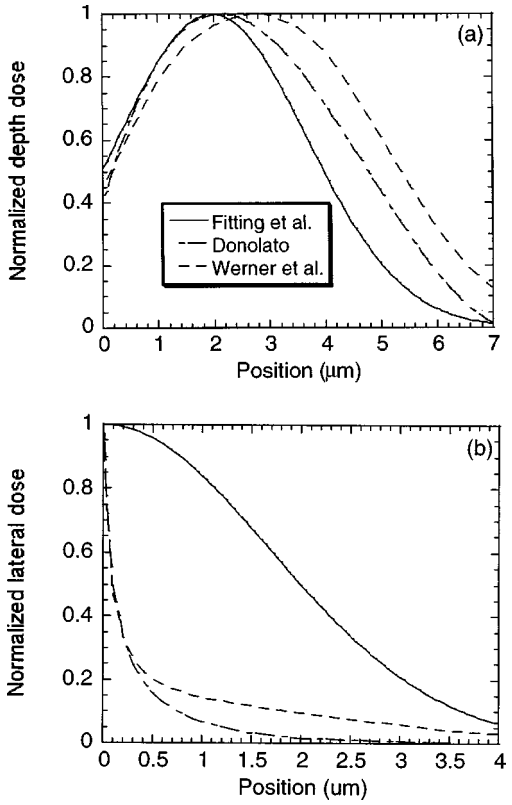

FIG. 3. (a) Depth dose and (b) lateral dose at 30 keV for three analytical models for the generation volume: spherical Gaussian model of Fitting *et al.* (see Ref. 20), Donolato's pear-shaped volume (see Ref. 21), and the analytical approximation to Monte Carlo results by Werner *et al.* (see Ref. 23).

ferent analytical approximations:[19] a point source (Appendix A), Fitting's[20] spherically-symmetrical Gaussian (Appendix B), Donolato's[21] pear-shaped (Appendix C), and von Roos and Luke's cubic[22] generation volume models. The normalized, integrated depth-dose and lateral-dose profiles for two of these models are shown in Fig. 3 for 30 keV beam energy and the corresponding profiles from an analytical approximation to Monte Carlo results[23] are included for comparison. It is clear from those curves that the more complicated pear-shaped profile agrees more closely with the Monte Carlo simulations than does the spherical Gaussian model. The point source was chosen as an example of a simpler scheme permitting relatively rapid calculation and the Gaussian and pear-shaped models were chosen as examples of more realistic models. The point-source model is used in this work in a rapid preliminary fitting process to produce initial estimates for the more sophisticated models. The cubic model is used as an independent check of results. It is beyond the scope of this article to make a detailed study of the validity of a wide range of generation models.

Figure 4 compares theoretical collection efficiency curves using the various generation models. As expected[22] the profiles are found to be similar except very close to the grain boundary (within 2 μm in our example).

B. Determination of grain boundary location

It is inappropriate to simply assume that the data point with minimum EBIC corresponds to the center of the grain boundary since EBIC measurements always include superimposed noise and since the profile is sampled discretely. In general, the location of the EBIC minimum is not precisely known. We considered the inclusion of the grain boundary location as an additional fitting parameter in the iterative procedure outlined below but rejected that approach for the reasons that it would be detrimental to speed and would add unnecessary complication. Instead, we simply performed a preliminary fit[24] of linear segments,

$$I \approx \begin{cases} a + m(x-d), & (x-d) < 0 \\ a - m(x-d), & (x-d) \geqslant 0 \end{cases},$$

to the EBIC data close to the grain boundary. The three fitting parameters, a, m, and d, correspond to approximations to the EBIC at the grain boundary, the gradient (assumed to be of equal magnitude each side), and the location of the grain boundary. The position scale of our data set was then adjusted to set $x_0 = 0$ at the center of the grain boundary for subsequent processing. A possible refinement of this procedure is to permit a different gradient in each grain.

Additionally, even in the absence of noise and sampling errors, the EBIC minimum may not coincide with the center of the grain boundary if the diffusion lengths in the grains either side differ significantly and the surface recombination velocity of the grain boundary is not very high.[22] The model of von Roos and Luke[22] was used, following our estimation of diffusion lengths and grain boundary recombination velocity, to check that no significant shifting of the EBIC minimum from the grain boundary center was to be expected in our case.

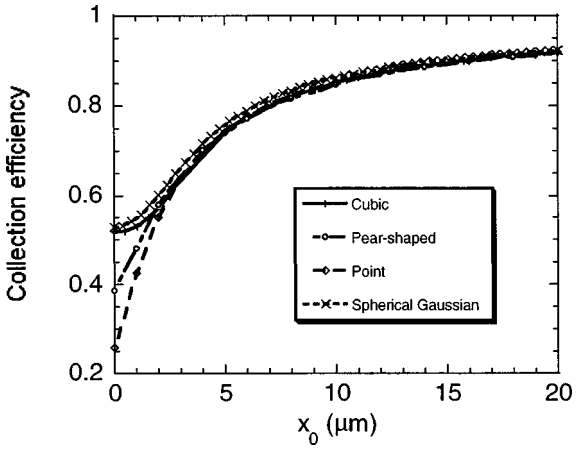

FIG. 4. Theoretical collection efficiency profiles, $\eta = I_0(1-c)$, for four generation volumes. Parameters in each case are: $L = 150\ \mu$m, $v_s = 4.5 \times 10^5$ cm s^{-1}, $D = 30$ cm^2 s^{-1}, $R = 6.6\ \mu$m. For the pear-shaped model, the beam diameter is assumed to be 50 nm. The I_0 value for the pear-shaped generation volume was used in converting contrast to collection efficiency for the spherical Gaussian generation.

C. Production of contrast profile

In order to convert an EBIC profile to a contrast profile, it is necessary to estimate the zero-EBIC level, i_{zero}, and the maximum EBIC level far from a grain boundary, $i_{\max}$. The contrast is then given by $c = (i_{\max} - i_{\text{raw}})/(i_{\max} - i_{\text{zero}})$, where the i_{raw} values are the original EBIC data. The zero-EBIC

level must be found by recording the measurement system's output when the electron beam is moved to a location where no EBIC is generated. In general, there is a different value for i_{max} in each grain if the diffusion lengths of the grains differ.[22] As has been pointed out elsewhere,[10,18] the determination of i_{max} is extremely critical for the determination of L and we followed the procedure suggested by Donolato and Bell[10] which involves fitting an exponential curve,

$$I(x_0) = i_{max} - Cx^n \exp(-\alpha x_0), \tag{4}$$

to each tail of the EBIC profile, where i_{max}, C, n, and α are fitting parameters. We set $n=0$ as was generally done by the earlier authors,[10] who found that the results were relatively insensitive to the value of n. Equation (4) was applied only to the data points within the range where the contrast was less than 0.15.[10]

D. Determination of *s* and *L*

A nonlinear regression program,[24] implemented in Turbo Pascal, was used to fit Eq. (1) to the contrast data. Rather than treat the data for each grain separately as proposed elsewhere[6] we chose to solve for the least-squares fit for both grains simultaneously with the following three fitting parameters: L_{left} and L_{right}, the diffusion length on the left and right sides, respectively, of the grain boundary and $s = v_s/D$. Such an approach ensures that the same value of s is used in calculations for both grains and that the procedure produces a unique estimate for the grain boundary recombination velocity. The approach of allowing a different L value in each grain follows Donolato[6] and von Roos and Luke[22] and differs from that taken by Mittiga *et al.*[25] in which asymmetries across the grain boundary were attributed to its obliqueness and the diffusion length was assumed to be the same in each grain. We intend to investigate these alternative causes of asymmetry with the aid of three-dimensional numerical modeling.[26]

Equation (1) has been shown[22] to be erroneous when the diffusion lengths on each side of the grain boundary are different and the grain boundary recombination velocity is small enough to permit significant carrier transport across to grain boundary. This was not of great importance in our example case since the grain boundary recombination velocity was high. However, it would be a useful extension of this work to use the expressions derived in Ref. 22 in a direct fitting procedure, particularly if that work could be extended to make use of a generation model more realistic than a cube of constant generation rate.

E. Injection level

The effective recombination velocity of a grain boundary is a function of local minority carrier concentration and, hence, of probe (beam) current, unless low injection conditions are maintained.[10,27–29] We experimentally confirmed a very small dependence of the grain boundary contrast on probe current at the level used in this work (see results below) but also applied the available theoretical models to estimate the peak minority carrier concentrations for comparison with the doping level. The models provide estimates appropriate for homogeneous material and would tend to overestimate the minority carrier concentration in the presence of enhanced recombination at the grain boundary.

We estimated the minority carrier density due to the electron beam by following Berz and Kuiken[30] and Donolato[31] in approximating the generation volume by a sphere of constant generation rate. The Berz and Kuiken expression for the maximum excess minority carrier concentration for long diffusion length, zero surface recombination velocity and for the generation sphere tangent to the surface is, $\Delta n_{max} = G/(2\pi Da)$, where G is the total generation rate (s^{-1}) and a is the sphere radius. The total generation rate[32] was estimated from $G = EI_b(1-f)/(qe_i)$, in which E and I_b are the beam energy and current, $f \approx 0.1$ is the fraction of incident electrons backscattered,[33] q is the electronic charge, and $e_i \approx 3.63$ eV is the average electron-hole pair production energy.[33,34] The sphere's radius, a, was assumed equal to half the penetration range,[31,35,36] $2a = 0.0171E^{1.75}$, where E is in keV and a in μm. Donolato's[31] plots of minority carrier concentrations for infinite diffusion length show maximum levels close to $\Delta n_{max} \approx ga^2/(3D)$, where $g = 3G/(4\pi a^3)$ is the uniform generation rate per unit volume within the sphere.

Elsewhere, Donolato[21] gives an expression by which the carrier concentration in the emitter resulting from his pear-shaped generation model may be calculated for arbitrary front surface recombination velocity. We obtained an upper limit for the minority carrier concentration in the base region from this expression by the use of two assumptions. First, the effect of the proximity of the junction on the reduction of carrier concentration was minimized by assuming in Donolato's expression that the emitter thickness was twice the primary electron range. Second, since the front surface of our base region is the collecting junction, we used in the Donolato expression an infinite front surface recombination velocity. Results from these models are tabulated in Sec. IV.

III. EXPERIMENT

The EBIC analysis was performed on a p-n junction solar cell made from cast polycrystalline silicon (Solarex/Wacker Chemitronic). The p-type base doping level was $\sim 10^{16}$ cm^{-3} and a shallow junction was formed by solid source phosphorus diffusion for 18 min at 820 °C, resulting in a measured top sheet resistivity of 150 Ω/square. A 1.3 μm thick aluminum rear contact was sintered and the front surface was oxide passivated at 850 °C for 10 min in oxygen and for 30 min in nitrogen atmosphere. The front contact grid of Ti, Pd, and Ag was applied by photolithography. The junction depth was confirmed to be less than 1 μm by observing EBIC while scanning the electron beam across the edge of the cell.

EBIC images were obtained using a Cambridge Instruments S-360 scanning electron microscope (SEM). This microscope has digital image acquisition and storage incorporated into the basic instrument. We interfaced our EBIC system directly to this data acquisition system by feeding the

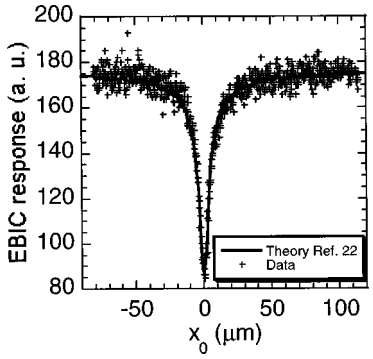

FIG. 5. EBIC data from scan across a grain boundary with scaled theoretical collection-efficiency profile (see Ref. 22).

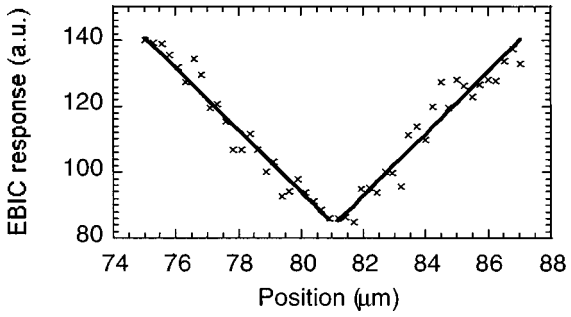

FIG. 6. Linear fit to EBIC data close to the grain boundary, used to ascertain the best fit to the location of the grain boundary.

output of a current-to-voltage converter (GW Electronics Type 31) into the SEM's video store to produce a 768×576 pixel image which was stored as an 8-bit Tagged Image File Format (TIFF) file for subsequent image processing. The overall linearity of this acquisition scheme was established by injecting known currents into the electrometer and examining the gray level of the corresponding image. The electrometer gain and offset were adjusted to ensure that both the baseline and maximum EBIC signal were maintained within the range of the SEM's video channel A/D converter. The electrometer baseline signal could be established by either blanking the electron beam or scanning the electron beam off the junction area. The electron gun, housed in a chamber pumped continuously with its own ion pump, uses a tungsten filament. The filament was initially saturated at the start of the day and EBIC measurements were normally conducted after more than five hours of operation in order to ensure stability of the electron probe current. The probe current was measured with a Faraday cup using a Keithley 486 Picoammeter. The drift of the probe current was determined to be approximately 0.2% per hour at a probe current of 100 pA. In order to establish low-injection conditions, the maximum grain boundary contrast was measured as the probe current was reduced. The lowest stable probe current that could be obtained on this SEM was measured at 1.3 pA. This was measured using the most sensitive range of the picoammeter and could have an absolute error of 20%–30%. EBIC images were recorded using an accelerating voltage of 30 kV, at probe currents of 1.3, 10, and 100 pA. A frame acquisition time of 320 s was used in order to reduce signal noise and also to ensure that a steady-state EBIC signal was recorded. The electron beam spot size was determined to be less than 0.05 μm by scanning the probe over a sharp edge. Line profile data for selected grain boundaries were extracted from the images using the public domain NIH Image program.[37] An improvement in the data acquisition system to reduce the noise level could be provided by an external computer with higher resolution A/D conversion and multiple sampling per pixel to allow recording the EBIC signal from single line scans without the need for subsequent image processing to extract data.

IV. RESULTS AND ANALYSIS

The example one-dimensional EBIC scan data, after correction for the zero level, are shown in Fig. 5. The scan consists of 765 points, spaced approximately 0.25 μm apart. The data are presented in arbitrary units, as recorded by the measurement system, since absolute current or collection efficiency is not required for the subsequent analysis. In addition, the beam current, necessary for calculation of collection efficiency, could not be accurately measured since the beam current being measured was only approximately 1% of the full scale of the meter. However, the beam current was monitored to gain assurance of its stability throughout the experiment.

Figure 6 shows the least-squares fit of two linear segments of equal absolute gradient to the data close to the grain boundary. That fit yielded an estimate of 81.06 μm for the position of the EBIC minimum from the start of the scan. We assume that the EBIC minimum coincides with the center of the grain boundary.

With the origin of the position scale shifted to the grain boundary the exponential expression of Eq. (4) was fitted to the ''tail'' of the profile on each side in order to estimate the asymptotic EBIC signal (I_0) which would be expected in each grain in the absence at the grain boundary. On the arbitrary scale of Figs. 5 and 6 the asymptotes were estimated to be 174.9 for the left-hand grain and 175.4 for the right-hand grain. There is a considerable degree of uncertainty associated with these values due to the superimposed noise and the consequences of this uncertainty are discussed below. The contrast data, found using these I_0 values in Eq. (3), are plotted in Fig. 7.

The fitting of theoretical contrast profiles by nonlinear regression was carried out using three different models for the generation volume: point source, symmetrical Gaussian, and pear-shaped (see Appendices). In the case of the point source, the data within 2 μm of the grain boundary were excluded from the fitting process since this generation is expected to produce an unrealistically sharp contrast profile in that region (Fig. 4). The fitted curves are shown with the grain boundary region data in Fig. 7. In this case the spherical Gaussian generation model produces the closest fit to the data points close to the grain boundary, while the contrast peak modeled with the pear-shaped model is sharper than in the data. At this stage we do not have a complete explanation

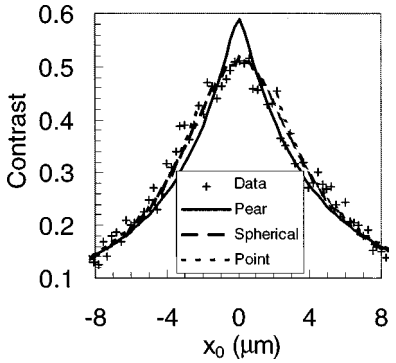

FIG. 7. Experimental contrast data and three theoretical least-squares approximations to it using different models for the generation volume: point source, spherical Gaussian and pear-shaped models. (b) is an expanded portion of (a).

for this discrepancy but it appears that the broader lateral spread of the spherical Gaussian source may allow a closer approximation to this experimental data set since it produces a more rounded peak in the contrast profile. We discounted the possibility that the excessive sharpness of the theoretical profile for the pear-shaped source is due to underestimation of the beam spot size, d, by calculating the contrast profile variation as d is changed (see Fig. 8). That suggested that such underestimation would need to be by a factor of approximately 30 to explain the result and our measurement was not so inaccurate. The resulting values for the three fitting parameters and their estimated fractional errors[24] are listed in Table I. Note that those fractional errors are for the numerical fitting process only and exclude errors in the estimation of the background current and the range-energy relationship (see Sec. V). A diffusion coefficient of 30 $cm^2\ s^{-1}$ was estimated for a p-type doping level of 10^{16} cm^{-3} by using the Einstein relation and an empirical approximation for electron mobility in single-crystal silicon.[38]

The results in Table I were checked with the von Roos–Luke formulation[22] for the collection efficiency across a grain boundary when the diffusion lengths on each side differ. Since the absolute collection efficiency data were unavailable, we used a scaling factor to allow for uncertainties in beam current, pair-production energy and backscatter coefficient and fitted the scaled theoretical collection efficiency to the measured EBIC (Fig. 5) in arbitrary units. Use of parameter values of $L_{\text{left}}=85\ \mu$m, $L_{\text{right}}=100\ \mu$m, and $v_s=6\times10^5$ cm s^{-1} was found to match the data well, as shown in Fig. 5.

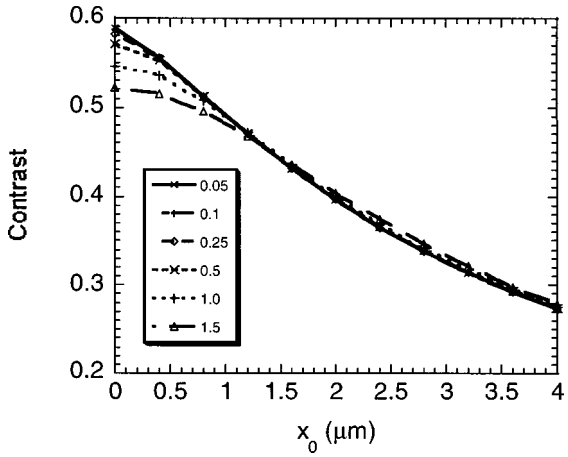

FIG. 8. Theoretical contrast profiles (pear-shaped generation model) for $L=100\ \mu$m, $v_s=4.0\times10^5$ cm s^{-1}, $D=30$ $cm^2\ s^{-1}$ with the beam spot size (μm) as plotting parameter.

TABLE I. Parameter values extracted by fitting theoretical grain boundary EBIC profiles using different models for the generation volume to an experimental profile. The v_s values were calculated from the actual fitting parameter, s, by the assumption of a diffusivity of $D=30$ $cm^2\ s^{-1}$. Note that the quoted uncertainties refer only to the numerical fitting process and exclude the much larger uncertainties associated with estimation of baseline current and choice of range-energy relationship. The results are listed in order of decreasing localization of the generation, leading to increasing values of the diffusion lengths.

Generation volume model	L_{left} (μm)	L_{right} (μm)	v_s (10^5 cm s^{-1})
Point source	44.6±0.3	95.6±0.7	6.30±0.04
Pear-shaped	52.1±2.6	108±9	4.07±0.04
Spherical Gaussian	54.6±1.6	131±5	8.01±0.06

V. DISCUSSION

A fundamental problem with the theory which underlies this work is the insensitivity of the calculated contrast profile to variations in the values of diffusion length used in the calculation when collection efficiency is high,[39] as would be expected in good quality solar cells. This comes about because when the diffusion length is long enough to produce a collection efficiency which approaches unity any increase in diffusion length makes little or no change to the collection

The results from the three methods for estimating the maximum minority carrier concentration for our experimental conditions (for $E=30$ keV and $I_b=1.3$ pA) are listed in Table II. Since the tabulated levels are far exceeded by the doping concentration, we can be confident that our sample was in low injection throughout. Confirmation that our results were almost independent of injection level was obtained by observation of the grain boundary contrast as a function of beam current. For each value of beam current, the beam was refocused to ensure a constant beam diameter. The peak contrast as a function of beam current is shown in Fig. 9, which indicates that there is only a very small variation in the measured contrast as a function of I_b for I_b close to the value used to produce the data of Fig. 6.

TABLE II. Theoretical estimates of peak minority carrier concentration in silicon in the absence of a grain boundary for a 1.3 pA beam of 30 keV electrons.

Method	Peak minority carrier concentration (cm^{-3})
Berz and Kuiken[a]	1×10^{12}
Donolato graph[b]	5×10^{11}
Donolato expression[c]	2×10^{12}

[a]Reference 30.
[b]Reference 31.
[c]Reference 21.

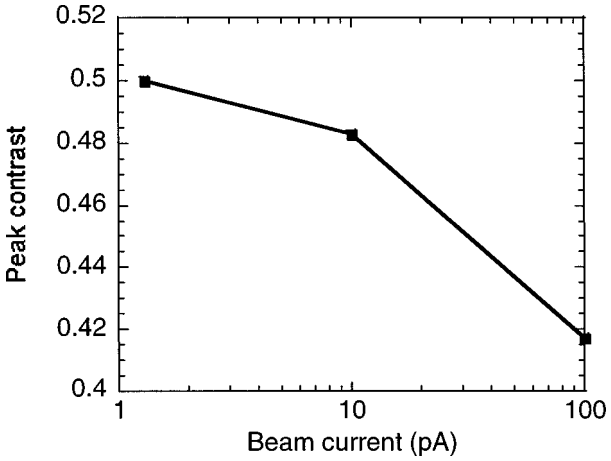

FIG. 9. Measured grain boundary contrast as function of beam current.

efficiency or to the collected current.[40] As has been noted elsewhere,[18] errors in the estimation of I_0 of the order of only 1% can generate errors in L exceeding 100%. In Fig. 10 we show contrast profiles calculated using the point-source model for a range of diffusion lengths with all other parameters held constant. The figure shows that for large values of L the contrast profiles converge and become difficult to distinguish from each other. Some alternative EBIC methods which might otherwise have been used to independently estimate diffusion length, such as the methods of Wu and Wittry[41] or Kittler and Schröder,[42] are prone to the same limitation. In addition, our estimates for I_0 are influenced by the presence of superimposed noise which derives from instrumentation noise, exacerbated by the very low beam current used here to ensure low injection conditions, and possibly from variable backscatter fraction due to surface roughness.[43] These experimental issues could, in principle, be avoided by slower scanning with enhanced averaging at each data point combined with careful surface polishing.

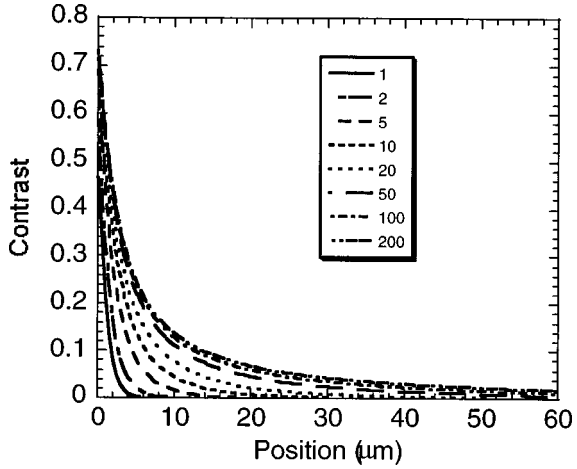

FIG. 10. The effect of diffusion length on theoretical contrast (point-source model). The plotting parameter is diffusion length (μm) and constants used in calculation of the curves were: $E=30$ keV, $v_s=4.5\times10^5$ cm s^{-1}, $D=30$ cm^2 s^{-1}.

However, it would remain difficult to obtain accurate estimates for diffusion lengths due to the very heavy reliance on baseline estimates.

Another source of uncertainty which is excluded from the errors indicated in Table I is associated with the choice of range-energy relationship. In this work, we have used the Everhart–Hoff[35] relationship exclusively yet Luke[44] has demonstrated that an alternative formulation due to Kanaya and Okayama[45] would have produced a 33% longer range estimate at 30 keV. Luke showed that a range difference of 85% could result in extracted surface recombination velocity values which differed by a factor of 3. Hence, although we have obtained good agreement (Table I) between the diffusion length measurements fitted using different generation volume models, it should be remembered that the same estimates for I_0 and the range were used in all cases and that small variations in those estimates could lead to large changes in the fitted values of L and the errors indicated in Table I, which exclude errors in I_0 and in the range, are substantially smaller than the overall errors.

The fitted v_s values are less sensitive than are diffusion lengths to the accurate estimation of the baseline but it is evident from our results in Table I that v_s depends quite strongly on the choice of the model for the generation volume. This is to be expected since v_s is strongly related to the form and magnitude of the contrast profile close to the grain boundary and it is in this region that the different generation models differ significantly (Fig. 4). Without a detailed examination of a large number of alternative generation models and experimental results of generation volume experiments, which is beyond the scope of this article, it is difficult to confidently state which of the sets of results in Table I is the most reliable. However, we tend to place most credibility in those which used the pear-shaped model since this model includes a Gaussian lateral dependence which broadens with increasing depth, a feature suggested by experiment[46] and theory.[47] Additionally, the pear-shaped model is in approximate agreement with a model derived from Monte Carlo results[23] (Fig. 3). This issue is further complicated by the fact that some experimental methods which have been used to characterize the generation volume have not discriminated between carrier generation and their subsequent diffusion.[48]

The check of the results in Table I against the von Roos/Luke theory[22] offers support for the recombination velocity values in Table I but the ratio of the diffusion length estimate on each side of the grain boundary is significantly less than in Table I. This difference is the subject of ongoing investigation. Our intention is to reduce noise in future experimental EBIC scans by modifying the experimental equipment to allow slow single scans in preference to the extraction of single scan data from two-dimensional images. Additionally, hardware improvements will be made to permit accurate measurement of small beam currents.

VI. CONCLUSION

We have discussed the limitations inherent in Donolato's integral-parameter method of extracting grain boundary recombination velocity and intragrain diffusion length from

EBIC scans across vertical grain boundaries and described and demonstrated our direct-fitting procedure which overcomes some of those limitations. In addition, we have discussed the inherent lack of reliability in the Donolato theory of fitted L values when the collection efficiency is high. It may be found in future work to be appropriate to estimate independently the diffusion length(s) and use the above fitting technique to find the grain boundary recombination alone. One way to estimate L independently may be by extended spectral analysis methods,[49] although it may be difficult to obtain values pertaining to individual grains rather than a spatial average. A promising avenue for future research is the use of three-dimensional simulation[26,50,51] to check the analytical theory within its range of applicability, explore the usefulness of the theory in cases which do not strictly meet the restrictions for its use, and to model complex arrangements of grain boundaries for which a comprehensive theory has not been developed.

ACKNOWLEDGMENTS

The Photovoltaics Special Research Center is supported by the Australian Research Council's Special Research Centres scheme and by Pacific Power. A.B.S. gratefully acknowledges the financial support of an Australian Research Council Postdoctoral Research Fellowship. R.C. thanks Dr. Jean-Marc Bonard and Dr. Anatoli Chtanov for helpful discussions. The authors are grateful for the assistance of Dr. Mel Dickson of the UNSW Electron Microscope Unit.

APPENDIX A: EVALUATION OF CONTRAST ASSUMING POINT-SOURCE GENERATION

The point-source contrast is given by

$$c(x_0)=Q^*/\exp(-z'/L),$$

where z' is the source depth and[52]

$$Q^*=\frac{2s}{\pi}\int_0^\infty\left[\frac{k\,\exp(-\mu|x_0|)\sin(kz')}{\mu^2(2\mu+s)}\right]dk.$$

The integration was performed numerically. The use of 10^{-1} and 10^6 in place of the true lower and upper limits of zero and infinity results in negligible error for this and the following generation models.

In the literature different assumptions have been made for the depth of sources (point, spherical, cubic). We compared $z'=\alpha R$ with[20,53] $\alpha=0.3$ and[30,54] 0.4 and used the latter since we found that it yielded contrast profiles in good agreement with the pear-shaped generation except very close to the grain boundary.[22] R is the primary electron range in silicon which has been approximated[35] as $R=0.0171E^{1.75}$ μm, where E is the beam energy in keV.

APPENDIX B: EVALUATION OF CONTRAST WITH SPHERICAL GENERATION MODEL

Fitting[20] describes a simple model, also used by Donolato,[55] for the spatial distribution of beam-generated carriers in the semiconductor. The concentration varies as a spherically-symmetrical Gaussian around a center at depth $z_0=0.3R$. Fitting's model for the generation volume is

$$h(x,z)=K\,\exp\{-\beta^2[x^2+(z-z_0)^2]\}$$

and $\beta^2=7.5R^{-2}$. The factor, K, need not be evaluated since it cancels in the contrast calculation.

The contrast is then given by

$$c(x_0)=\frac{2Ks}{\pi I_0}\int_0^\infty\left(\frac{k}{\mu^2(2\mu+s)}\int_0^\infty\{\sin(kz)\times\exp[-\beta^2(z-z_0)^2]\}dz\int_{-\infty}^\infty\{\exp(-\mu|x|)\times\exp[-\beta^2(x-x_0)^2]\}dx\right)dk.$$

The x integral has an analytical solution which is found by treating the negative and positive ranges separately,[56]

$$\int_{-\infty}^\infty\exp[-\mu|x|-\beta^2(x-x_0)^2]dx=\frac{\sqrt{\pi}}{2\beta}\exp\left(\frac{\mu^2}{4\beta^2}\right)\sum_{n=0,1}\left\{\exp[(-1)^n\mu x_0]\times\operatorname{erfc}\left[\frac{\mu}{2\beta}+(-1)^n\beta x_0\right]\right\}.$$

The z integral may also be solved analytically,[57,55]

$$\int_0^\infty\{\sin(kz)\exp[-\beta^2(z-z_0)^2]\}dz=-i\sqrt{\pi}/(4\beta)\exp(-\beta^2z_0^2)\sum_{n=0,1}[(-1)^n\times\exp(\Gamma)\operatorname{erfc}(2\beta\Gamma)],$$

where $\Gamma=-[2\beta^2z_0+(-1)^nik]/(4\beta^2)$ and the integral is real for real values of the input parameters. A numerical approximation to the complex error function due to Salzer[58] has been reproduced in a standard reference.[59] The outer, k, integration must be performed numerically. The background current is

$$I_0=\frac{A\pi}{2\beta^2}\exp\left[(4\beta^2L^2)^{-1}-\frac{z_0}{L}\right]\operatorname{erfc}[(2\beta L)^{-1}-\beta z_0].$$

The integrated depth- and lateral-dose profiles are proportional to $\exp[-\beta^2(z-z_0)^2]$ and $\exp[-\beta^2(x-x_0)^2]$, respectively.

APPENDIX C: EVALUATION OF CONTRAST ASSUMING PEAR-SHAPED GENERATION VOLUME

Donolato[21] describes a pear-shaped generation volume whose width depends on the beam's spot size, d, on the sample surface. The spot size is defined as the diameter of a circle which circumscribes half the beam current. The generation is given by

$$g(r,z)=\frac{g_0\Lambda(z)}{2\pi R\sigma^2(z)}\exp\left[\frac{-r^2}{2\sigma^2(z)}\right],$$

where $r^2=x^2+y^2$, $\sigma^2(z)=0.36d^2+0.11z^3/R$ is the lateral variance of the distribution and[31]

$$\Lambda(z)=\begin{cases}0.6+6.21z/R-12.4(z/R)^2+5.69(z/R)^3, & 0\leqslant z/R\leqslant 1.1\\ 0, \quad \text{elsewhere}\end{cases}$$

describes the integrated depth dose. Applying Eq. (2) yields

$$h(x-x_0,z)=\frac{g_0\Lambda(z)}{(2\pi)^{1/2}R\sigma(z)}\exp\left[\frac{-(x-x_0)^2}{2\sigma^2(z)}\right].$$

By separating the inner (x) integral of Eq. (1) into its negative and positive ranges, an analytical solution[57] may be found:

$$\frac{g_0\Lambda(z)}{(2\pi)^{1/2}R\sigma(z)}\int_{-\infty}^{\infty}\exp(-\mu|x|)\exp\left[\frac{-(x-x_0)^2}{2\sigma^2(z)}\right]dx$$

$$=\frac{g_0\Lambda(z)}{2R}\sum_{n=0,1}\left\{\exp\left[\frac{\mu}{2}(\mu\sigma^2(z)+(-1)^n 2x_0)\right]\right.$$

$$\left.\times\operatorname{erfc}\left[\frac{\sigma(z)[\mu+(-1)^n x_0/\sigma^2(z)]}{\sqrt{2}}\right]\right\}$$

The background current is[60]

$$I_0=g_0/R\int_0^{1.1R}\Lambda(z)\exp(-z/L)dz=g_0/R[34.14L^4R^{-3}$$

$$-24.8L^3R^{-2}+6.21L^2R^{-1}+0.6L+\exp(-1.1R/L)$$

$$\times(-34.14L^4R^{-3}-12.754L^3R^{-2}+0.4153L^2R^{-1}$$

$$-0.00039L)].$$

The factor g_0 need not be evaluated since it cancels in Eq. (1). The z and k integrations in Eq. (1) must be performed numerically.

The integrated lateral dose (Fig. 3) may be found by numerical integration of $h(x-x_0,z)$ over z from zero to $1.1R$. The integrated depth dose is given by $\Lambda(z)$.

[1] L. Kazmerski, Renewable and Sustainable Energy Reviews **1**, 71 (1997).
[2] W. Palz and H. Zibetta, in *Yearbook of Renewable Energies 1992*, edited by W. Palz (Ponte, Bochum, Germany, 1992), p. 181.
[3] M. Y. Ghannam, Renewable Energy, **6**, 601 (1995).
[4] M. A. Green, Diffus. Defect Data, Part B **51-52**, 509 (1996).
[5] Z. Chen, R. J. Matson, and L. C. Burton, Phys. Status Solidi A **132**, 51 (1992).
[6] C. Donolato, J. Appl. Phys. **54**, 1314 (1983).
[7] C. Donolato, J. Appl. Phys. **54**, 1314 (1983), Eq. (30).
[8] C. Donolato, J. Appl. Phys. **54**, 1314 (1983), Eq. (12).
[9] C. Donolato, J. Appl. Phys. **54**, 1314 (1983), Eqs. (26) and (28).
[10] C. Donolato and R. Bell, Rev. Sci. Instrum. **54**, 1005 (1983); **55**, 133 (1984).
[11] B. Raza and D. B. Holt, in *Microscopy of Semiconducting Materials 1995*, edited by A. G. Cullis and A. E. Staton-Bevan (IOP, Bristol, 1995), p. 107.
[12] F. Battistella and A. Rocher, Semicond. Sci. Technol. **2**, 226 (1987).
[13] A. Mittiga and M. Cappizzi, J. Appl. Phys. **62**, 3443 (1987).
[14] C. H. Seager, J. Appl. Phys. **53**, 5968 (1982).
[15] J. D. Zook, Appl. Phys. Lett. **37**, 223 (1980).
[16] K. Masri, J. P. Boyeaux, S. N. Kumar, L. Mayet, and A. Laugier, Mater. Res. Soc. Symp. Proc. **106**, 89 (1988).
[17] J. Marek, J. Appl. Phys. **55**, 318 (1984).
[18] H. Field and D. Ast, J. Appl. Phys. **64**, 955 (1988).
[19] E. B. Yakimov, Bull. Russ. Acad. Sci. Phys. **56**, 312 (1992).
[20] H. J. Fitting, H. Glaefeke, and W. Wild, Phys. Status Solidi A **43**, 185 (1977).
[21] C. Donolato, Phys. Status Solidi A **65**, 649 (1981).
[22] O. von Roos and K. L. Luke, J. Appl. Phys. **55**, 4275 (1984).
[23] U. Werner, F. Koch, and G. Oelgart, J. Phys. D **21**, 116 (1988), Eqs. (5)–(8).
[24] M. S. Caceci and W. P. Cacheris, BYTE **9** (5), 340 (1984).
[25] A. Mittiga, M. Capizzi, C. Coluzza, A. Frova, V. Parisi, D. Cavalcoli, L. Moro, and M. Prudenziati, J. Appl. Phys. **63**, 4748 (1988).
[26] R. Corkish, T. Puzzer, A. B. Sproul, K. L. Luke, and G. Heiser, in Proceedings of Solar '97, Canberra, 1997, edited by T. Lee (Australian and New Zealand Solar Energy Society, 1997).
[27] C. H. Seager, J. Appl. Phys. **52**, 3960 (1981).
[28] R. Sudarena and J. G. Fossum, J. Appl. Phys. **56**, 964 (1984).
[29] O. Breitenstein and J. Heydenreich, *In Situ Scanning Electron Microscopy in Materials Research*, 1st ed. (Akademie, Berlin, 1995), Chap 7, pp. 127–156.
[30] F. Berz and H. K. Kuiken, Solid-State Electron. **19**, 437 (1976).
[31] C. Donolato, Optik (Stuttgart) **52**, 19 (1978/79).
[32] Eu. Yakimov, Scanning Microsc. **6**, 81 (1992).
[33] J. I. Hanoka and R. O. Bell, Annu. Rev. Mater. Sci. **11**, 353 (1981).
[34] R. D. Ryan, IEEE Trans. Nucl. Sci. **NS-20**, 473 (1973).
[35] T. E. Everhart and P. H. Hoff, J. Appl. Phys. **42**, 5837 (1971).
[36] A. Romanowski and A. Buczkowski, Solid-State Electron. **28**, 645 (1985).
[37] Computer code, NIH Image (U.S. National Institutes of Health and available on the Internet at ⟨http://rsb.info.nih.gov/nih-image⟩).
[38] D. M. Caughey and R. E. Thomas, Proc. IEEE **55**, 2192 (1967).
[39] C. Donolato (personal communication).
[40] This point is evident from the steepness of the curve of diffusion length versus charge collection efficiency published by L. W. Snyman, H. C. Snyman, and J. A. A. Engelbrecht, J. Appl. Phys. **59**, 1216 (1986).
[41] C. J. Wu and D. B. Wittry, J. Appl. Phys. **49**, 2827 (1978).
[42] M. Kittler and K.-W. Schröder, Phys. Status Solidi A **77**, 139 (1983).
[43] A. B. Sproul, T. Puzzer, and R. B. Bergmann, Proceedings of Second World Conference on Photovoltaic Solar Energy Conversion, Vienna, Austria, July 6–10, 1998 (to be published).
[44] K. L. Luke, J. Appl. Phys. **76**, 1081 (1994).
[45] K. Kanaya and S. Okayama, J. Phys. D **5**, 43 (1972).
[46] A. Cohn and G. Caledonia, J. Appl. Phys. **41**, 3767 (1970).
[47] R. W. Nosker, J. Appl. Phys. **40**, 1872 (1969).
[48] J.-M. Bonard, J.-D. Ganière, B. Akamatsu, D. Araújo, and F.-K. Reinhart, J. Appl. Phys. **79**, 8693 (1996).
[49] P. A. Basore, *Proceedings of the 23rd IEEE Photovoltaic Specialists Conference*, Loiusville, KY (IEEE, New York, 1993), pp. 147–152.
[50] M. Stemmer, Mater. Sci. Eng., B **24**, 180 (1994).
[51] N. Tabet and M. Ledra, Mater. Sci. Eng., B **42**, 181 (1996).
[52] C. Donolato J. Appl. Phys. **54**, 1314 (1983), Eq. (23).
[53] K. L. Luke, J. Appl. Phys. **80**, 5775 (1996).
[54] K. L. Luke and O. von Roos, Solid-State Electron. **26**, 901 (1983).
[55] C. Donolato, Mater. Sci. Eng., B **24**, 61 (1994).
[56] I. S. Gradshteyn, I. M. Ryzhik and A. Jeffery, *Table of Integrals, Series, and Products*, 5th ed. (Academic, San Diego, 1994), Eq. 3.322(2); the corresponding expression for the negative range was found using the Mathematica computer package.
[57] Ref. 56, Eq. 3.897(1).
[58] H. E. Salzer, Math. Tables Aids Comp. **5**, 67 (1951).
[59] M. A. Abramowitz and I. A. Stegun, *Handbook of Mathematical Functions* (Dover, New York, 1972), Eq. 7.1.29.
[60] C. Donolato J. Appl. Phys. **54**, 1314 (1983), Eq. (26).